

Thermal and Thermo-mechanical Properties of Poly(ethylene terephthalate) Nanocomposites

Jayita Bandyopadhyay, Suprakas Sinha Ray[†], and Mosto Bousmina*

National Centre for Nanostructured Materials, Council for Scientific and Industrial Research Materials Science and Manufacturing, PO Box 395, Pretoria 0001, Republic of South Africa

*Department of Chemical Engineering, Laval University (CREPEC), Quebec G1K 7P4, Canada

Received December 5, 2006; Accepted March 13, 2007

Abstract: In this study poly(ethylene terephthalate) (PET)/clay nanocomposites with two different weight percentages of montmorillonite (MMT) have been prepared by melt-extrusion technique. The X-ray diffraction (XRD) patterns and transmission electron microscopic (TEM) images reveal the formation of intercalated nanocomposites. The melting and crystallization behaviors of neat polymer and nanocomposite samples have been investigated by using both conventional and temperature modulated differential scanning calorimetry (TMDSC). The DSC results for compression molded samples after cooling show successive melting with an endothermic peak accompanied by a shoulder for nanocomposite samples. This is due to the presence of two different sizes of crystallites. DSC and TMDSC results for quenched samples show melting is followed by cold crystallization and in this state initial percent of crystallinity present in nanocomposite samples are higher than that of neat PET sample. For all samples, TMDSC results also confirm the melting is associated with re-crystallization phenomenon. The dynamic mechanical analyses (DMA) show in all temperature range, noticeably in the higher temperature region the nanocomposites exhibit tremendous improvement of modulus; but the slight difference in clay content doesn't effect significantly. The thermogravimetric analyses (TGA) reveal the overall thermal stability of PET matrix slightly improves after nanocomposite preparation.

Keywords: poly(ethylene terephthalate), nanocomposite, thermal and thermo-mechanical properties

Introduction

Over past two decades, one of the most prospective fields of research in industries and academia is the preparation to processing of polymer nanocomposites. After pioneering report from the Toyota research group on Nylon-6 (N6)/montmorillonite (MMT) nanocomposite [1], a new field of research, known as layered silicate based polymeric nanocomposites is developing very rapidly. It has been established that the incorporation of a few weight percent of layered silicate enhances the properties of virgin polymer concurrently [2]. Up to this date almost all types of polymers have been used for the preparation of nanocomposites with layered silicates [2-4]. In the family of thermoplastic polyester resins, poly(ethyl-

ene terephthalate) (PET) is well known for its world wide application as a food and beverage container with low cost and high performance plastic. Depending on its processing condition and thermal history, PET resin may exist in amorphous state as well as in semi-crystalline state. Its slow crystallization rate and high melting temperature make it advantageous for packaging industries. The primary objective of preparation of PET/clay nanocomposites is to improve the gas barrier properties of neat polymer. Because layered silicates are believed to increase the barrier properties by creating a maze or 'tortuous path' that retards the progress of the gas molecules through the matrix resin [5,6].

The main objective of this work is to prepare and investigate the thermal and thermo-mechanical properties of PET/OMLS nanocomposite and to understand the effect of filler concentration on those properties. For this purpose PET/Closite 20A (organically modified montmor-

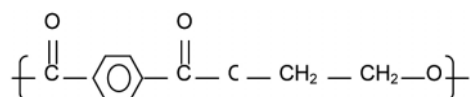
[†] To whom all correspondence should be addressed.
(e-mail : RSuprakas@csir.co.za, bousmina@gch.ularal.ca)

illonite, commercial name C20A) nanocomposites with two different weight percents of layered silicate have been prepared. Then melting behaviors of above mentioned samples in different states have been studied by both conventional (DSC) and temperature modulated differential scanning calorimetry (TMDSC). The thermo-mechanical properties have been studied for neat polymer and corresponding nanocomposites. The thermal stability measurements of neat PET and various nanocomposite have also been carried out.

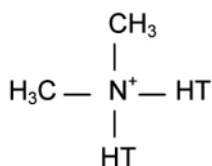
Experimental

Materials

The PET (commercial name Vitiva) used for this study was supplied by Eastman Chemical Company. The chemical structure of the polymer is given below



The organoclay Cloisite[®] 20A (C20A) was purchased from the Southern Clay Products. It is a natural montmorillonite (MMT) modified by dimethyl dihydrogenated tallow quaternary ammonium salt with cation exchange capacity of 95 meq/100 g [7]. The molecular formula of the surfactant is given below



The polar solubility parameters (δ) for PET and organic modifier of C20A were estimated roughly from group contribution method of Fedors [8] and values are 24.3 and 16.9 J^{1/2}cm^{-3/2} respectively. Although these δ values are not close to each other, however, we selected this combination because of high thermal stability of the surfactant of as received C20A compared to other cloisite clays and larger gap between the silicate layers (2.45 nm, estimated from the XRD result). To determine the thermal stability of C20A at the processing condition, the sample was kept at 270 °C for 5 min and it showed ~4 % weight loss. All of these materials were dried at 110 °C for 24 h under vacuum before blending to avoid degradation caused by moisture.

Nanocomposite Preparation

Nanocomposites were prepared by melt extrusion in Haake twin screw extruder at a screw speed of 30 rpm,

barrel temperatures used were 260 °C, 270 °C, 270 °C and temperature of die was 270 °C. After collecting nanocomposite samples from extruder they were dried under vacuum at 110 °C for 24 h to remove the water and then molded under several conditions according to the needs of different experiments. Initially the samples were molded by using a Carver laboratory press at 280 °C, under 2MPa pressure for 2 min and the sample thickness were ~1.2 mm. In order to study the thermal properties in the amorphous state by DSC Q100 instrument, the samples (sealed within the DSC pans) were kept at 280 °C for ~20 min for complete melt and to remove all previous thermal history and then quenched in liquid nitrogen.

Characterization Techniques and Property Measurements

X-Ray Diffraction (XRD) analyses ($2\theta = 0 \sim 30^\circ$) were performed by a Simens-500 diffractometer under transmission mode. The beam was Cu K α ($\lambda = 0.154$ nm) operated at 40 KV, 40 mA. Dispersability of the clay platelets in the PET matrix was determined by means of Transmission Electron Microscope (TEM, JEOL model JEM 1230 instrument). The samples were epoxy mounted and ultramicrotomed with a diamond knife. The sample thicknesses were kept within a range 50 ~ 70 nm.

The melting and crystallization kinetics were studied by differential scanning calorimeter (DSC model: TA Q100). For conventional DSC the temperature and energy readings were calibrated with Indium and for TMDSC the heat capacity was calibrated with sapphire sample. In order to observe the melting behavior of compression molded samples, heating and cooling tests were carried out at a heating and cooling rate of 20 °C/min from 0 to 290 °C. The amount of sample utilized for these tests were within the range 6.3 ~ 6.5 mg. To investigate the melting and crystallization phenomena of the amorphous state in detail both conventional and modulated DSC experiments were performed. Here sample weights were varied between 3.5 ~ 4.3 mg. The standby temperature of the DSC cell was sated to 20 °C prior to start experiments and the quenched samples were placed in the DSC cell as quickly as possible in both DSC and TMDSC from liquid nitrogen. For conventional DSC the scan rate was 20 °C/min in the temperature window of 30 ~ 300 °C. In TMDSC the samples were examined at a heating rate of 5 °C/min in the scan window of 30 ~ 300 °C with modulation amplitude ± 0.796 °C every 60 s.

The dynamic mechanical analyses (DMA) for the compression molded samples were carried out by using Rheometric Scientific Analyzer within the temperature range 0 ~ 180 °C with a heating rate 2 °C/min and strain 0.02 %.

The thermo gravimetric analyses (TGA) were carried

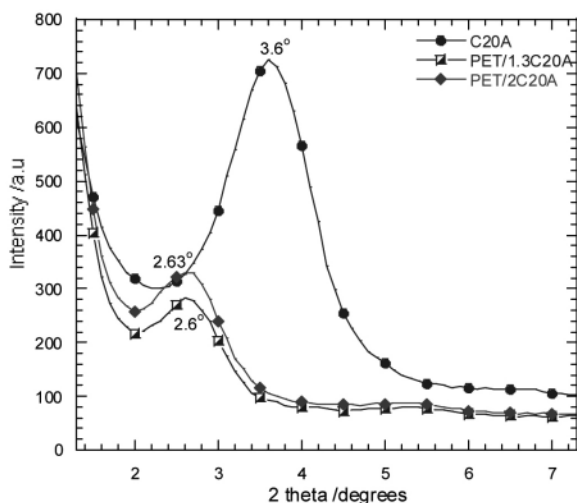


Figure 1. Small angle X-Ray Diffraction patterns (XRD) of organoclay and nanocomposites with two different wt% of organoclay.

out by using TA Q500 instrument in the temperature range 0~900 °C under both air and nitrogen atmospheres. The amounts of silicate present in nanocomposite samples were also determined by using TGA. According to TGA analysis, the amount of inorganic part present in the first batch nanocomposite was 1.3 % and that in the second batch nanocomposite was 2 % and hence the nanocomposites were abbreviated as PET/1.3C20A and PET/2C20A respectively.

Results and Discussion

Nanocomposite Structure

The most common tool to probe the structure of the nanocomposite is XRD. Figure 1 shows the XRD patterns of pure C20A powder and nanocomposites (compression molded samples of thickness 1 mm) in the lower angle region. The characteristic (001) peak of C20A powder appeared at $2\theta = 3.6^\circ$ ($d = 2.45$ nm). For nanocomposite samples the characteristic peak intensity of C20A was not only significantly reduced due to the dilution effect of clay but also shifted at $2\theta = 2.6^\circ$ ($d = 3.39$ nm) and $2\theta = 2.63^\circ$ ($d = 3.36$ nm) for PET/1.3C20A and PET/2C20A nanocomposites respectively. These peak shifts towards the lower angle side indicated the intercalation of polymer chains inside the clay galleries.

To support the XRD observations, TEM analyses were carried out. Parts a and b of Figure 2 respectively represents the TEM images of PET/1.3C20A and PET/2C20A nanocomposites. The intercalated clay layers can be directly visualized by the black entities in TEM images [9]. Although some clay agglomerates are still exists, however, most of them were well dispersed in the PET

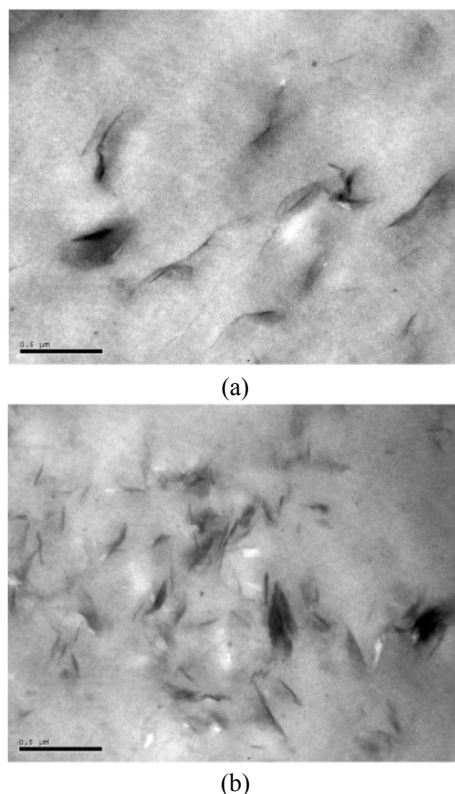


Figure 2. Bright field Transmission Electron Microscopic (TEM) images of (a) PET/1.3C20A and (b) PET/2C20A nanocomposites. The black entities representing the boundaries intercalated clay layers.

matrix. The inhomogeneous dispersion of clay layers can be attributed to the less favorable interaction between the polymer matrix and the C20A surface.

Melting Behavior

As Received PET and as Prepared Nanocomposite Samples

To elucidate the melting behavior of the neat polymer and the effect of incorporation of nano-filler to it with different percentages, DSC tests were first performed at a heating and cooling rate of 20 °C/min within the scan window of 20 to 290 °C. The DSC thermograms of first heating, cooling and second heating are respectively represented in parts a, b, and c of Figure 3. The different measurable quantities are tabulated in Table 1. During the first heating cycle, the T_g of both nanocomposite samples were accompanied by enthalpy relaxation. Since some initial crystallinity was present in all samples or even when the sample was in amorphous state, one can generally consider the existence of some disordered arrangements, lacking of a long range order, and the presence of some short range structures [10], at the glassy state those structures try to attain a new equilibrium condition which results such enthalpy relaxation. Further increase in temperature resulted cold crystallization (in

Table 1. DSC Results for as Received and as Prepared Samples (from Cooling and Second Heating Run)

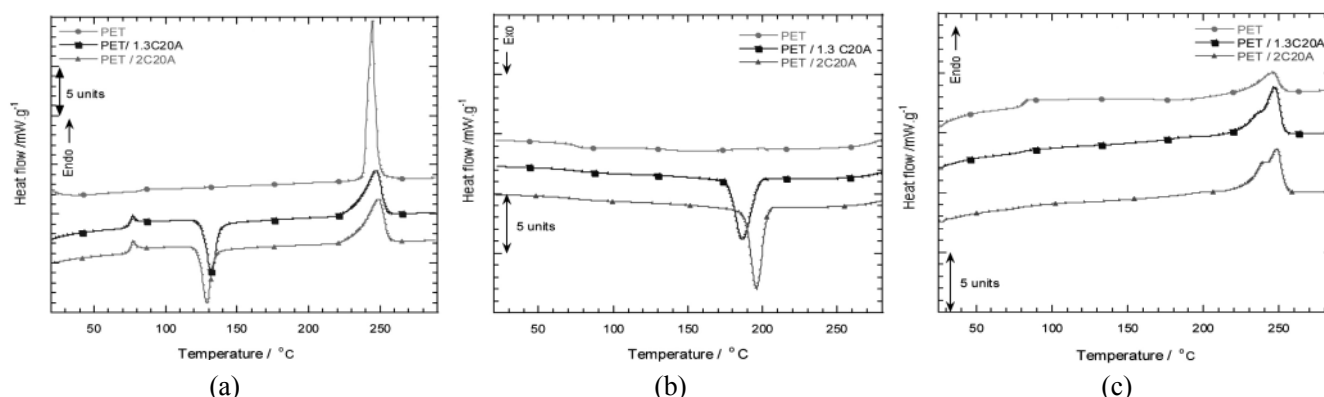
Sample	T_g	$T_{m,on}$	T_m	ΔH_f	T_c	ΔH_c
PET	82.41	189.07	245.24	26.32	156.65	6.36
PET/1.3C20A	78.97	201.52	246.71	48.62	186.62	50.70
PET/2C20A	79.11	209.12	248.01	46.24	195.96	51.72

Table 2. DSC Results for as Prepared Compression Molded Samples (from Cooling and Second Heating run)

Sample	T_g	$T_{m,on}$	T_m	ΔH_f	T_c	ΔH_c
PET	80.55	209.69	247.48	30.91	174.47	23.10
PET/1.3C20A	80.57	216.80	249.51	32.11	200.77	40.51
PET/2C20A	81.65	215.02	249.41	32.61	199.51	39.54

Table 3. DSC Results for Melt-quenched (in liquid nitrogen) Samples

Sample	T_g	T_{cc}	ΔH_{cc}	T_m	ΔH_f	% crystallinity
PET	78.65	159.15	51.35	248.18	54.62	2.33
PET/1.3C20A	76.57	124.57	45.28	247.77	58.91	9.73
PET/2C20A	74.76	121.27	45.30	248.44	60.66	10.96

**Figure 3.** DSC thermograms of as received PET and as prepared nanocomposites during: (a) first heating from 20 to 290 °C, (b) cooling from 290 to 20 °C and (c) second heating from 20 to 290 °C at a rate 20 °C/min.

nanocomposites) and then melting.

According to Figure 3b, during cooling the shift of crystallization peak temperature (T_c) toward higher temperature and increase in heat of crystallization (ΔH_c) for nanocomposites compared to PET indicate that the nucleation mechanism is responsible here for the growth of crystals in nanocomposites. Further a small variation of clay content didn't show a significant change of ΔH_c values.

The T_g reported in Table 1 are of second heating scan presented in Figure 3c. The T_g shifted towards the low temperature in nanocomposites, but remained almost unchanged with increase in clay content. This may be due to the degradation of polymer matrix at the processing temperature. To support this it is necessary to have a look on T_g s of PET in Table 1, 2, and 3. The T_g reported in Table 1 is of as received PET sample. The com-

pression molding resulted a decrease in T_g value (as reported in Table 2). During melt-quenching the neat PET was treated thermally in a confined environment before quenching, which resulted a further reduction of T_g value (as reported in Table 3). Henceforth, it can be concluded the matrix polymer degraded in different levels depending on the way of thermal treatment and in nanocomposites the surfactant residing on the surface of the organoclay stimulated this phenomena. The melting peak temperature (T_m) and heat of fusion (ΔH_f) followed the same trend as T_c and ΔH_c .

Compression Molded Samples

To study the melting behavior of the compression molded polymer and nanocomposite samples, DSC tests were first performed at a heating rate of 20 °C/min. The DSC thermograms of first cooling and second heating are rep-

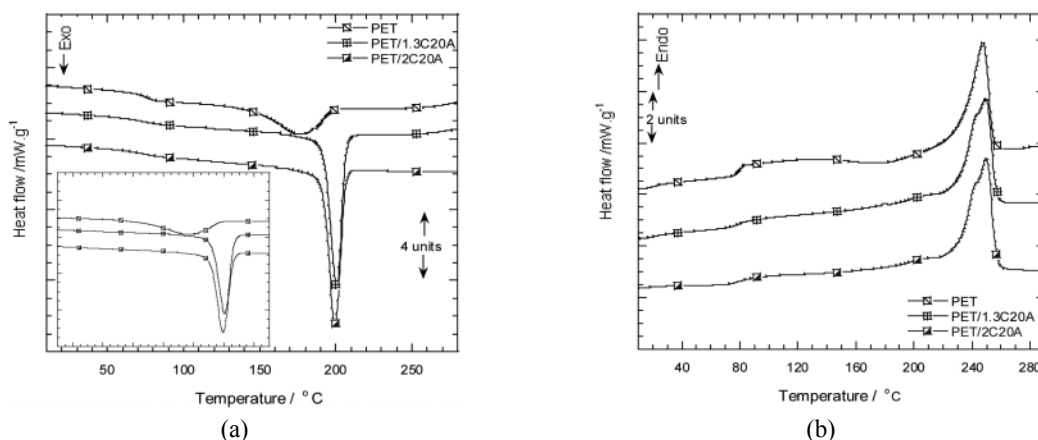


Figure 4. DSC thermograms of compression molded (at 280 °C) samples of neat PET and nanocomposites during: (a) cooling from 290 °C and (b) subsequent heating at a rate 20 °C/min.

resented in Figures 4a and b respectively. The different measurable quantities are tabulated in Table 2.

According to Figure 4a and Table 2, for both nanocomposites the crystallization peak temperatures (T_c) were shifted towards the higher temperature range and the heat of crystallization (ΔH_c) were increased compared to the pure polymer. Further, with increase in clay content, the values of T_c and ΔH_c were slightly decreased compared to PET/1.3C20A nanocomposite. These findings indicate that incorporation of C20A enhanced the crystallization mechanism of neat PET and this enhancement is more important with low clay content.

In the subsequent heating scans, as shown in Figure 4b, the glass transition temperature (T_g) of neat PET was not altered after the addition of C20A. This indicates C20A has almost no favorable interaction with PET matrix. During compression molding, the mobility and orientation of polymer chains along with clay platelets differ from the as prepared nanocomposites. Probably, because of this reason, the T_g s remained almost unaltered in nanocomposites compared to PET as reported in Table 2. On the other hand, a slight deviation from the base line can be observed in PET thermogram just before melting. This exothermic deviation may be due to the presence of some non-crystalline materials after first cooling, which under goes further crystallization during melting [11]. All of these crystals (formed during cooling and subsequent heating) melted at around 247.5 °C. Upon heating, instead of appearing a single melting endotherm like PET; a shoulder melting endotherm was appeared in both nanocomposite samples. This may be due to the presence of either imperfect or small size crystallites. The melting peak temperatures reported in Table 2 are of clearly distinguishable melting endotherm. Here increase in melting peak temperature (T_m) and heat of fusion (ΔH_f) can be observed in both nanocomposites as compared to those

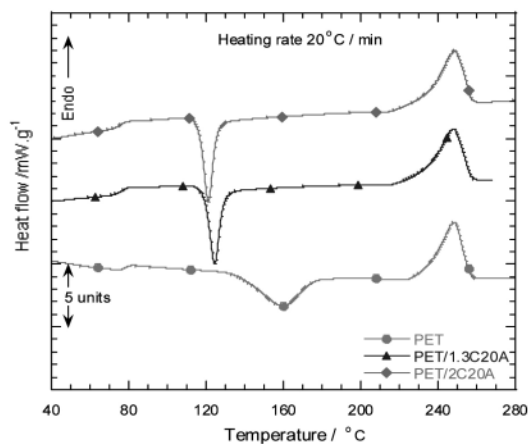


Figure 5. DSC thermograms of melt quenched samples of neat PET and nanocomposites. In order to get the melt quenched state, the samples sealed within DSC pans were melted at 280 °C for 20 min and then quenched in LN₂. The standby temperature of the DSC cell was maintained at 20 °C prior to start the experiment. The quenched samples were placed within the DSC cell as early as possible and the heating scan was performed within the scan window 30-300 °C at a scan rate 20 °C/min.

of neat PET sample. However, the incorporation of clay percentage has almost no effect on T_m and ΔH_f . Again, both nanocomposite samples showed higher onset of melting temperature ($T_{m, on}$) than neat PET sample. Since $T_{m, on}$ is related to the stability to melting, therefore, according to Table 2 one can say it increased in nano composites and higher clay content results a little decrease in melting stability.

Melt Quenched Samples

Since the PET resin exhibits different properties in amorphous and semi-crystalline state, the crystallization behavior of both PET and nanocomposites in or near the

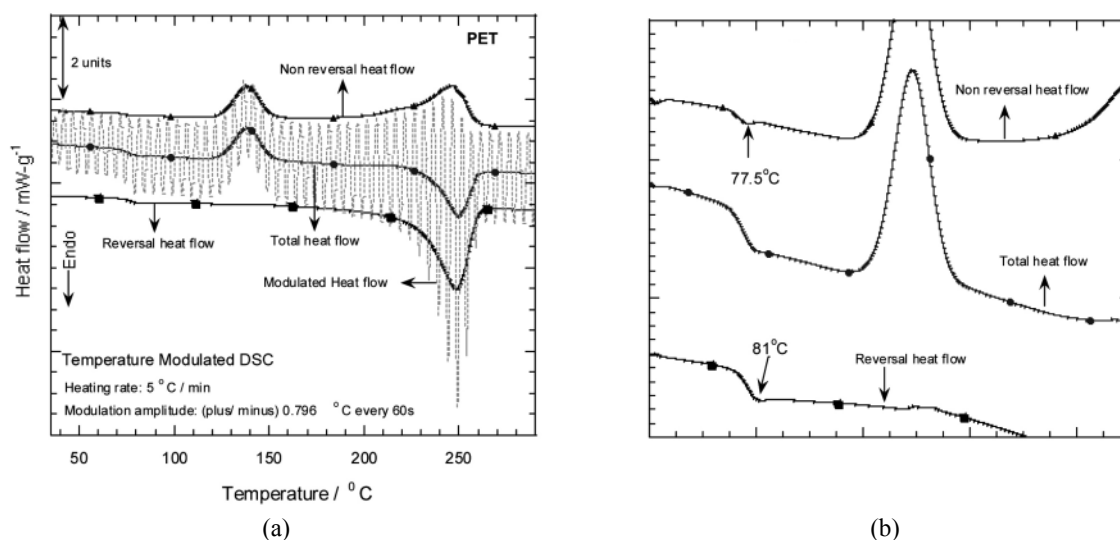


Figure 6. Temperature Modulated DSC traces of quenched samples of: (a) PET, (b) enlarged view of Figures (a). Here also in order to prepare the melt quenched samples, the samples sealed within DSC pans were melted at 280 °C for 20 min and then quenched in LN₂. The standby temperature of the DSC cell was maintained at 20 °C prior to start the experiment. Those samples were examined at a heating rate of 5 °C/min in the scan window of 30~300 °C with modulation amplitude ± 0.796 °C every 60 s.

Table 4. TMDSC Results for Melt-quenched (in Liquid Nitrogen) Samples

Sample	T_g	T_{cc}	ΔH_{nonrev}		ΔH_{rev}	% crystallinity
			ΔH_{cc}	$\Delta H_{recryst}$		
PET	74.84	138.4	33.67	75.27	135.6	19.03
PET/1.3C20A	72.87	114.03	32.72	70.49	134.2	22.12
PET/2C20A	72.28	113.24	31.85	69.01	132.9	22.87

amorphous state were also studied. For this purpose, DSC and TMDSC were performed on specially prepared samples (as mentioned in experimental section) under the specific experimental conditions as explained in the characterization part. Figure 5 shows the DSC curves of melt quenched samples. The thermal parameters estimated from the thermograms are tabulated in the Table 3.

The T_g for all samples appeared clearly. The well-defined T_g is due to the removal of constraints that were provided by the crystallites in the initial material. The T_g of neat polymer shifted very slightly to the lower temperature in case of both nanocomposites. This may be due to the degradation of matrix upon addition of C20A during the removal of thermal history before quenching.

After T_g , with increase in temperature all of the three samples undergo crystallization before melting. The cold crystallization peak temperature (T_{cc}) of neat PET sample shifted systematically towards the lower temperature range with clay loading, indicating clay particles act as nucleating agent to start cold crystallization earlier. However, enthalpy of cold crystallization (ΔH_{cc}) of neat PET decreased in nanocomposites, it can be inferred that although clay acts as nucleating agent, nanocomposites lose their crystallizable moieties due to the intercalation

of some polymer chains in the clay galleries.

Figure 5 also shows during melting a single melting peak appeared for all three samples and the melting peak temperatures remained almost the same. But enthalpy of fusion (ΔH_f) increased in nanocomposites. Since ΔH_{cc} decreased in nanocomposites, it was expected that ΔH_f will also decrease. To find out the reason of increased ΔH_f in nanocomposites, the percent of crystallites present initially in the samples were calculated. To do this, the value of ($\Delta H_f - \Delta H_{cc}$) was divided by the heat of fusion of 100 % crystalline polymer (ΔH_f for 100 % crystalline PET = 140.1 mW/g) [12] and then multiplied by 100. According to Table 3 initial percent of crystallinity in nanocomposites was higher, i.e. they were not fully amorphous. For this reason ΔH_f in nanocomposites increased although ΔH_{cc} decreased.

To understand the detail melting and crystallization phenomena of all samples, TMDSC was also employed. TMDSC is the most useful tool to separate the heat flow into reversal and non-reversal kinetic components which offers more information about that process. Parts a, c, and d of Figure 6 respectively represents TMDSC thermograms of PET, PET/1.3C20A, and PET/2C20A nanocomposites and results are summarized in Table 4.

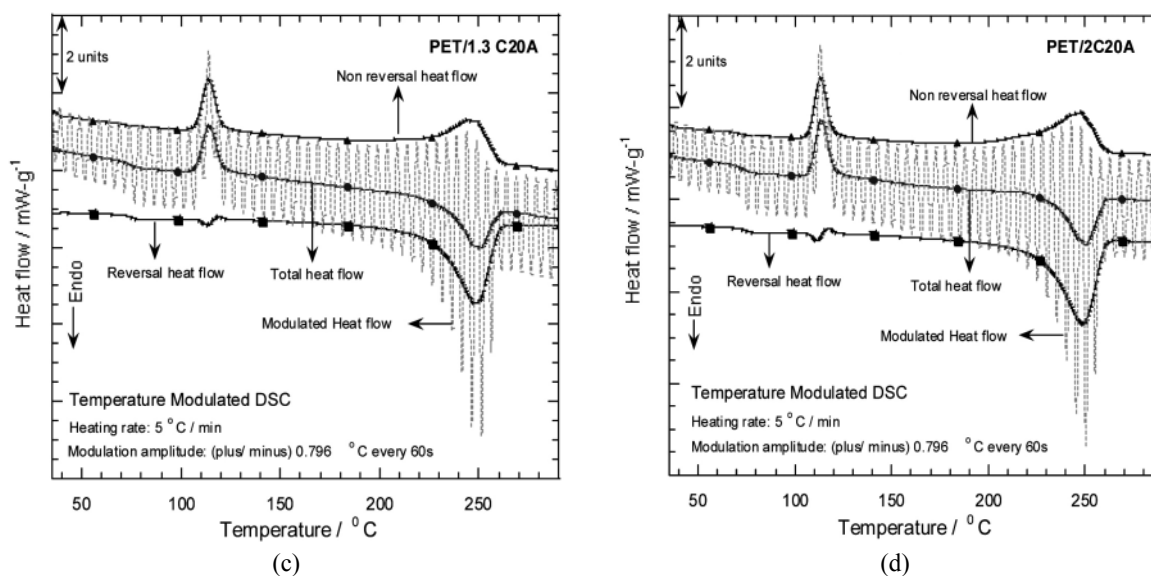


Figure 6 (continue). TMDSC traces of quenched samples of (c) PET/1.3 C20A nanocomposite and (d) PET/2 C20A nanocomposite.

As reported in Table 4, T_{cc} and ΔH_{cc} showed the same trend as conventional DSC measurements for quenched samples. But according to Figures 6c, and d, i.e. for nanocomposites, the cold crystallization is accompanied by a little fusion and subsequent crystallization in the reversal component. The probable reason is some shorter polymer chains were formed due to the degradation of matrix at high temperature in presence of surfactant. These small chains undergo a little fusion during the crystallization of the bulk.

According to Figures 6a, c, and d the melting phenomenon is associated with the melting (reversible component) and re-crystallization (nonreversible component) processes [13]. A single melting peak was observed for all samples. Here the percent crystallinity of each sample was determined from the following equation: % crystallinity = $\Delta H_{rev} / (\Delta H_{cc} + \Delta H_{recryst}) / 140.1$; where ΔH_{rev} is the area under the melting endotherm on the reversible cycle, ΔH_{cc} and $\Delta H_{recryst}$ is the area under the cold crystallization and re-crystallization exotherms on the non-reversible cycle. The initial degree of crystallinity (%) present in quenched samples from TMDSC (Table 4) was higher than that for conventional DSC (Table 3); but followed the same trend. Since the degree of crystallinity depends on many factors such as draw ratio between the rolls during collection of samples from extruder [13], inhomogeneous dispersion of clay in the polymer matrix etc., under the same conditions of preparing amorphous samples the deviation of results are possible.

The T_g reported in Table 4 were determined from the total heat flow. From the reversible and nonreversible heat flow traces of Figure 6b, i.e. in PET sample some structural relaxation or enthalpy of relaxation was followed by T_g .

Dynamic Mechanical Analysis

The parts a, b, and c of Figure 7 represent respectively the storage modulus (E'), viscous modulus (E'') and $\tan \delta$ values for PET and its two nanocomposites. The most interesting feature observed from these Figures is that, a sudden drop of both moduli for the virgin polymer since it became too soft as soon as it crossed the T_g . Where as, the existence of E' and E'' values at higher temperature, i.e. the presence of elasticity and plasticity in the nanocomposites at higher temperature can be explained by the reinforcement effect of organoclay after glassy state [14].

From Figure 7a it is clear that, below T_g , the magnitude of E' for PET/1.3C20A nanocomposite decreased very slightly compared to PET and increase in clay content results a further decrease in E' . According to Figure 7b and c, the magnitudes of E'' and $\tan \delta$ were also decreased compared to PET. The small interaction between the matrix and the filler is probably responsible for the reduction of the peak values of the storage and the viscous modulus.

Again, the temperature corresponding to the E'' and $\tan \delta$ peak were sifted towards higher temperature after addition of organoclay in the matrix resin. But there is no significant change with slight increase in organoclay loading. This feature can be explained as the introduction of filler to the polymer matrix reducing the segmental mobility of the polymer chains and as a result, the glassy state for the nanocomposites appeared at higher temperature compared to neat polymer. This result shows the same trend as the T_g determined for the compression molded samples by the DSC analysis.

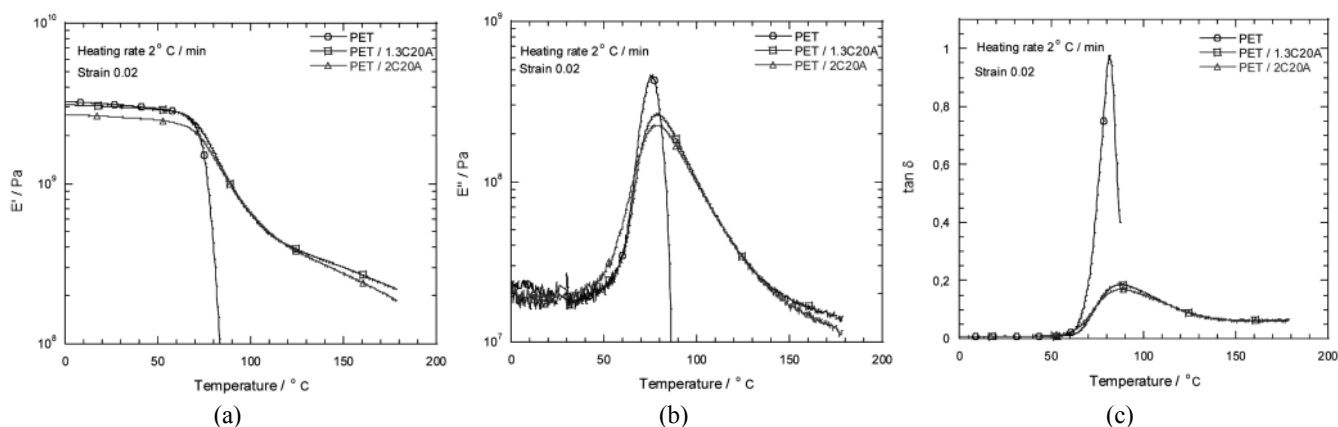


Figure 7. (a) Elastic modulus (E'), (b) viscous modulus (E'') and (c) $\tan \delta$ for PET and its nanocomposites. The DMA were carried out within the temperature range 0-180 °C with heating rate 2 °C/min and strain 0.02 %.

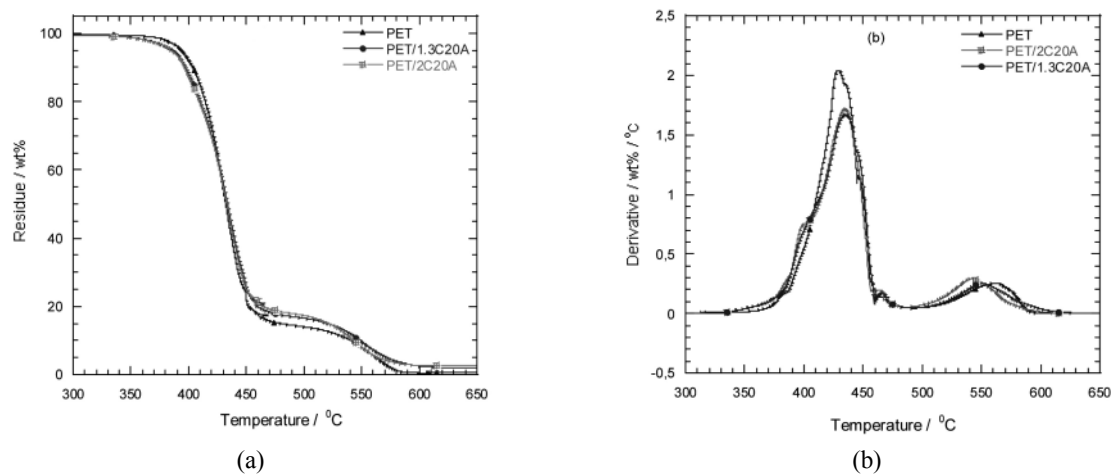


Figure 8. TGA analyses of (a) PET and (b) PET/clay nanocomposites under air atmosphere at heating rate 10 °C/min.

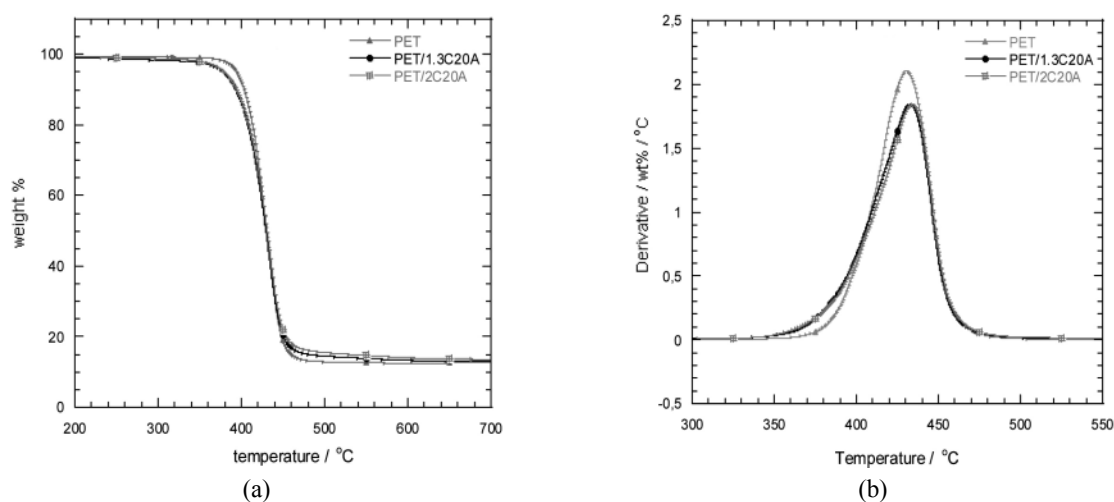


Figure 9. TGA analyses of (a) PET and (b) PET / clay nanocomposites under Nitrogen atmosphere at heating rate 10 °C/min.

Thermogravimetric Analysis

In this section the thermal stability of neat PET and nanocomposites in different atmospheres is discussed.

The TGA traces of the neat PET and nanocomposite samples in pyrolytic and thermo-oxidative conditions are presented in Figures 8 and 9, respectively. The onset

Table 5. Data from TGA Analyses

Sample	Onset Degradation (~10 % weight loss) Temperature	
	Under Air	Under Nitrogen
PET	402.03	404.17
PET-3C20A	396.25	393.06
PET-5C20A	395.28	394.44

degradation temperature (at 10 % weight loss) values of all samples in different atmospheres are summarized in Table 5. The first derivative TGA (dTGA) curves are also shown in Figures 8b and 9b. The dTGA curves are chosen for the presentation because they more clearly show the difference in thermal stability between samples. Under oxidative condition all samples exhibited two steps decomposition. In the first half of degradation process, nanocomposites exhibited less onset thermal stability than pure PET. This is due to the degradation of surfactant used for the modification of MMT [15,16], as alkyl ammonium modifiers are known to undergo Hoffman degradation around 200 °C [17]. However, the overall thermal stability of PET was increased after nanocomposite preparation with OMMT. This is due to the dispersion of intercalated silicate layers in the PET matrix, which by nature has higher thermal stability.

On the other hand, in inert atmosphere all samples exhibited single decomposition step as illustrated in parts a and b of Figure 9. Like oxidative condition, under inert atmosphere nanocomposite samples also exhibited less onset (at 10 % weight loss) thermal stability than that of neat PET. However, the main degradation temperature for the nanocomposite samples were increased in air compared to nitrogen atmosphere. It is possible that the different types of char formation mechanism under oxidative environment, actually slow down the oxygen diffusion, thus hindering the oxidation procedure under thermo-oxidative conditions. This observation indicates improved flame retardance property of the nanocomposite.

Conclusions

In this article we have systematically investigated the effect of organically modified montmorillonite on the melting, non-isothermal crystallization behaviours, and the thermal stability of neat PET. The nanocomposites with two different weight percentages of OMMT were prepared by melt-extrusion in twin-screw extruder. The XRD patterns and TEM observations established the formation of intercalated nanocomposites. The melting and crystallization behaviors of both neat PET and nanocomposite samples were investigated by both conventional and temperature modulated DSC. Results indicate

OMMT acts as a nucleating agent for the crystallization of PET.

To find out the effect of OMMT on the cold crystallization phenomenon of neat PET, conventional DSC and TMDSC of melt-quenched samples were also carried out. In nanocomposites the cold crystallization phenomenon was accompanied by a small fusion and subsequent crystallization in the reversal component during TMDSC. This may be due to the presence of some short polymer chains formed by the degradation of matrix at high temperature in the presence of OMMT. These small chains undergo a little fusion during the crystallization of the bulk. The shift of T_{cc} of PET toward lower temperature in nanocomposites suggested intercalated silicate layers act as nucleating agent to start the crystallization of matrix faster. However, the decreased in ΔH_{cc} of nanocomposites confirmed the fact although clay acts as nucleating agent, nanocomposites lose some crystallisable moiety due to the intercalation of polymer chains in the clay galleries. The further increase in temperature resulted melting with re-crystallization. In quenched state initial percent of crystallinity present in nanocomposites were higher than that in PET.

DMA results showed that for neat PET, both the storage and the loss modulus dropped suddenly just after T_g ; whereas the elastic and plastic behaviors are prominent in nanocomposites even at higher temperature due to the reinforcement effect of organofiller. The shift of the $\tan \delta$ peaks of the nanocomposites toward higher temperature can be attributed due to the increase in restricted segmental mobility of the polymer chain in the nanocomposites.

The TGA analyses showed although the degradation started earlier in nanocomposites due to the Hoffman degradation of the surfactant present in the organoclay, the average stability (indicated by the derivative curves) increased in nanocomposites. In air atmosphere nanocomposite samples showed higher stability than nitrogen atmosphere. This may be due to the different type of char formation mechanism under oxidative environment which actually slow down the oxygen diffusion, thus hindering the oxidation procedure under thermo-oxidative conditions. This observation indicates improved flame retardance property of the nanocomposite.

References

1. A. Okada, M. Kawasumi, A. Usuki, Y. Kozima, T. Kurauchi, and Y. Kamigaito, *MRS Symposium Proceedings*, Pittsburgh 1990;171: 45.
2. (a) S. Sinha Ray and M. Okamoto, *Prog. Polym. Sci.*, **28**, 1539 (2003); (b) J. H. Sung, M. S. Cho, H. J. Choi, and M. S. Jhon, *J. Ind. Eng. Chem.*, **10**, 1217 (2004); (c) S. Sinha Ray and M. Biswas *M. Adv.*

- Polym. Sci.*, **155**, 167 (2001).
3. S. Sinha Ray and M. Bousmina, *Prog. Mater. Sci.*, **50**, 962 (2005)
 4. (a) S. Sinha Ray, *J. Ind. Eng. Chem.*, **12**, 811 (2006); (b) A. Maiti and M. Biswas, *J. Ind. Eng. Chem.*, **12**, 311 (2006); (c) H. B. Kim, C. H. Lee, J. S. Choi, B. J. Park, S. T. Lim, and H. J. Choi, *J. Ind. Eng. Chem.*, **11**, 769 (2005); (d) F. F. Fei and H. J. Choi, *J. Ind. Eng. Chem.*, **12**, 843 (2006).
 5. D. J. Sekelik, S. Stepanov Enazarenko, D. Schiraldi, A. Hiltner, and E. Baer, *J. Polym. Sci. Part B: Polym. Phys.*, **37**, 847 (1999).
 6. S. Sinha Ray, K. Yamada, M. Okamoto, and K. Ueda, *Nano. Lett.*, **2**, 1093 (2002).
 7. Data sheet of Southern Clay Products, Inc. (<http://www.nanoclay.com>)
 8. D. W. V. Krevelen DWV. Properties of polymers. Amsterdam, The Netherlands: Elsevier (1990).
 9. S. Sinha Ray, K. Yamada, M. Okamoto, A. Ogami, and K. Ueda, *Chem. Mater.*, **15**, 1456 (2003).
 10. I. K. Moon and Y-H. Jeong, *Pure & Appl. Chem.*, **11**, 2321 (1997).
 11. I. E. Phang, K. P. Pramoda, T. Liu, and C. He, *Polym. Intern.*, **53**, 1282 (2004).
 12. Data sheet of PET from Perkin Elmer.
 13. S. Solarski, M. Ferreira, and E. Devaux, *Polymer*, **46**, 11187 (2005).
 14. S. Sinha Ray, K. Okamoto, and M. Okamoto, *J. Appl. Polym. Sci.*, **102**, 777 (2006).
 15. W. Xie, Z. Gao, W-P. Pan, D. Hunter, A. Singh, and R. Vaia, *Chem. Mater.*, **13**, 2979 (2001).
 16. W. Xie, Z. Gao, K-L. Liu, W-P. Pan, R. Vaia, D. Hunter, and A. Singh, *Thermochim. Acta*, **367**, 339 (2000).
 17. S. Sinha Ray, M. Bousmina, and K. Okamoto, *Macromol. Mater. Eng.*, **290**, 759 (2005).